Thermal conductivity of $UNi_{0.5}Sb_2$ single crystal

2006 J. Phys.: Condens. Matter 18 3097

(http://iopscience.iop.org/0953-8984/18/11/015)

INSTITUTE OF PHYSICS PUBLISHING JOURNAL OF PHYSICS: CONDENSED MATTER

J. Phys.: Condens. Matter **18** (2006) 3097–3105 doi:10.1088/0953-8984/18/11/015

Thermal conductivity of $UNi_{0.5}Sb_2$ single crystal

J Mucha, H Misiorek, R Troć and Z Bukowski

W Trzebiatowski Institute for Low Temperature and Structure Research, Polish Academy of Science, PO Box 1410, 50–950 Wroclaw 2, Poland

E-mail: r.troc@int.pan.wroc.pl

Received 3 November 2005, in final form 14 February 2006
Published 1 March 2006
Online at stacks.iop.org/JPhysCM/18/3097

Abstract

The thermal conductivity of a single crystal of $UNi_{0.5}Sb_2$ has been measured in the temperature range between 5 and 300 K. We find a large anisotropy in the thermal conductivity, which may be explained by the very large difference in the a and c lattice parameters. The thermal conductivity $\lambda_{ab}(T)$ measured within the ab plane was found to have absolute values considerably higher than that (λ_c) measured along the c axis. The former exhibits at 25 K a pronounced non-symmetric maximum with an absolute value of about 6 $W\,K^{-1}\,m^{-1}$ and an almost symmetric minimum at $T_N = 161$ K. The electronic heat transport, λ_e, was also derived from the Wiedemann–Franz law along these two crystallographic directions. Attempts to estimate the bipolar (λ_{bip}) and magnon (λ_{mag}) contents to the measured total thermal conductivity have been done. An analysis of the thermal conductivity data has been performed for both magnetically ordered and non-ordered states.

1. Introduction

The uranium diantimonides $UTSb_2$ (T = 3d-, 4d-, 5d-electron transition metal) crystallize with a simple tetragonal structure of the $HfCuSi_2$ type (space group $P4/nmm$) [1]. Preliminary magnetic and Mössbauer measurements have been performed previously on powder samples [2, 3]. Most of these compounds have been found to order magnetically at low temperatures and have been characterized as semimetallic Kondo lattices. One of this group of uranium ternaries, $UNiSb_2$, exhibits an antiferromagnetic ordering below $T_N = 175$ K [2, 3]. The ^{121}Sb Mössbauer investigation [3] has allowed the determination of the magnetic structure of this Ni-containing compound to be of AFII type with the magnetic moments being aligned along the crystallographic fourfold axis in the sequence $(+\,-\,-\,+)$ of ferromagnetic (001) planes, and with the magnetic unit cell being doubled along this axis with respect to the chemical one. The elongation of the magnetic unit cell along the tetragonal [001] direction causes flat Brillouin zones which produce cylindrical highly corrugated Fermi surfaces along [001] [4]. Such quasi-two-dimensionality features observed

recently in some groups of compounds, such as for example $UTGa_5$ [5], have attracted wide attention. Furthermore, a moment arrangement implies a uniaxial anisotropy and thus any directional measurements of the bulk properties of single crystals seem especially interesting. Recently we have succeeded in growing single crystals of selected $UTSb_2$ ternaries, among them the Ni-containing one [6]. It turned out that both the crystal structure refinement from the single crystal x-ray data and the EDX analysis have indicated a large deficiency on the crystallographic Ni atom sites, yielding the composition $UNi_{0.5}Sb_2$ [6]. Systematic studies, such as magnetic susceptibility, magnetization, electrical resistivity, magnetoresistivity, Hall effect, thermoelectric power, specific heat, and isothermal magnetocaloric effect measurements have been performed on such crystals [6–8]. For example, the established value of the normal Hall coefficient R_0 yields in the single-band model the concentration of free carriers corresponding to 0.55 electrons per formula unit [7]. Magnetic measurements of the oriented crystals along the main crystallographic axes [6] heave revealed more complex behaviours compared to those found on the polycrystalline sample [2]. Among others probably the order–order phase transition takes place at $T_{tr} = 64$ K, i.e. much below the Neél temperature $T_N = 161$ K [7]. The latter temperature, due to some crystallographic disorder caused by Ni atom deficiency, turned out to be about 14 K lower than that reported for the polycrystalline sample [2, 3]. At T_{tr} the results indicate a first-order character of this transition and suggest its spin-reorientation nature [7].

In this paper we present the results obtained in thermal conductivity measurements performed for cases of application of the temperature gradient along two main crystallographic directions, i.e. within the *ab* plane and along the *c* axis.

2. Experimental details

Single crystals of $UNi_{0.5}Sb_2$ were grown from a Sb flux as described in [6]. The crystals had the form of thin platelets of typical dimensions $5 \times 5 \times 1$ mm^3 with the *c* axis perpendicular to their surfaces. Bar-shaped specimens for physical measurements were cut from oriented bulk single crystals using a wire saw.

The thermal conductivity was measured using the stationary heat flux method in the temperature range 5–300 K. The experimental setup and the measurement procedure have been described in detail in [9, 10]. The temperature gradient along the sample was in the range 0.1–0.5 K. Particular care was taken to avoid a parasitic heat transfer between the sample and its environment. The measurement error was below 2% and the surplus error estimated from the scatter in the measurement points did not exceed 0.3%.

3. Results and discussion

Any analysis of the obtained results of the thermal conductivity in $UNi_{0.5}Sb_2$ is complex due to the presence in this compound at least two magnetic phase transitions; there may also be a structural one (see [6]). The thermal conductivity of $UNi_{0.5}Sb_2$ is plotted in figure 1 against temperature within the range 5–300 K. This is plotted for two temperature gradients: parallel to the *ab* plane and along the *c* axis. The anisotropy apparent in this figure is also demonstrated in table 1 in the form of the ratio λ^{ab}/λ^{c}.

As one can infer from this figure, the thermal conductivity in the temperature range T_N–300 K diminishes proportionally to $T^{0.53}$ and $T^{2.25}$, as measured in the *ab* plane (λ^{ab}) or along the *c* axis (λ^{c}), respectively. In the ordered state, λ^{ab} increases exponentially as $\exp(T/230)$ down to the temperature $T_{max} \approx 25$ K. Below this temperature the thermal conductivity λ^{ab} varies with temperature in other way, namely as $T^{0.62}$. A complete different

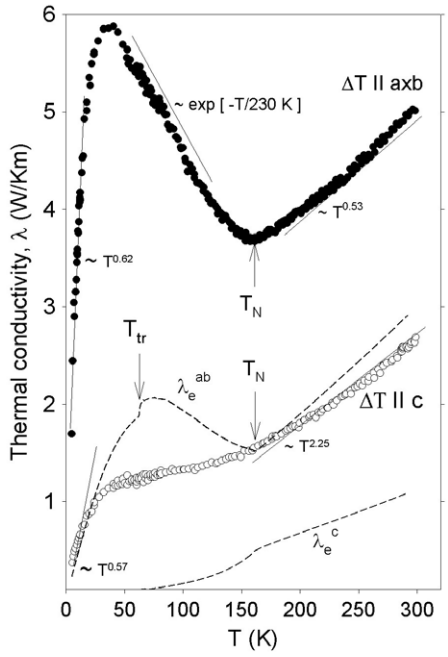

Figure 1. Thermal conductivity λ as a function of temperature measured with the temperature gradient ΔT applied parallel and perpendicular to the c axis. The straight lines drown through the experimental points show power or exponential temperature dependences. The dashed curve indicates the electronic thermal conductivity λ_e calculated by the Wiedemann–Franz law derived for both main crystallographic directions.

Table 1. Thermal conductivity anisotropy at various temperatures.

T (K)	10	50	100	150	200	250	300
λ^{ab}/λ^{c}	6.25	4.74	3.45	2.54	2.18	2.04	1.88

temperature dependence with respect to $\lambda^{ab}(T)$ is followed by $\lambda^{c}(T)$, which decreases in the entire temperature range below T_N.

According to classical theory of the heat transport of metals, semimetals or semiconductors [11], the electron thermal conductivity λ_e may be calculated from the Wiedemann–Franz law: $\lambda_e = L_0 T/\rho$, where L_0 is the Sommerfeld value ($L_0 = 2.44 \times 10^{-8}$ W Ω K^{-2}), ρ is the measured electrical resistivity (performed on the same samples) and T is the temperature. The electronic total thermal conductivities $\lambda_e^{ab}(T)$ and $\lambda_e^{c}(T)$, calculated from the above law, are presented in figure 1 by the dashed curves.

For the magnetic semimetals the total thermal conductivity, λ_{tot}, can be expressed as follows:

$$\lambda_{tot} = \lambda_{ph} + \lambda_e + \lambda_{bip} + \lambda_{magn} \tag{1}$$

where λ_{ph}, λ_e, λ_{bip} and λ_{magn} are the phonon, electronic, bipolar and magnon contributions.

In figure 2 we present the temperature variation of the difference $\Delta(\lambda_{tot} - \lambda_e)$. For pure dielectrics one can describe the phonon thermal conductivity as a simple kinetic expression $\lambda_{ph} = \frac{1}{3} C_v \nu \Lambda$, where C_v is the specific heat of a given dielectric, and ν and Λ are the mean velocity and mean free path of phonons. All the elements occurring in the expression

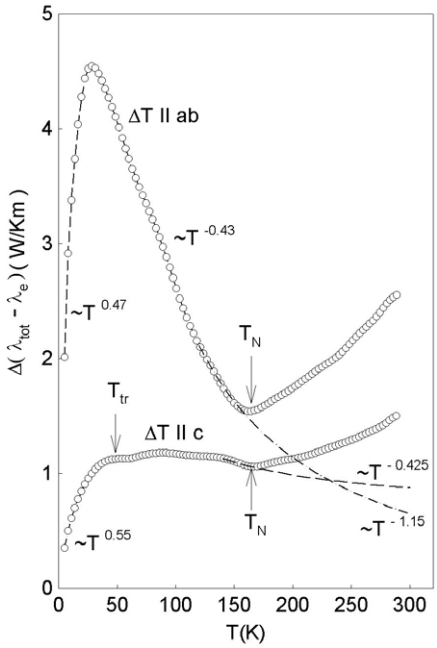

Figure 2. The difference $\Delta(\lambda_{\mathrm{tot}} - \lambda_{\mathrm{e}})$ estimated for two main crystallographic directions, i.e. parallel and perpendicular to the c axis, by subtracting from the total thermal conductivity λ_{tot} the electronic part λ_{e}. The approximate power dependences of the temperature are also shown. The dash–dotted and dashed curves show interpolations to higher temperatures of the low-temperature variations of the difference $\Delta(\lambda_{\mathrm{tot}} - \lambda_{\mathrm{e}})$ to estimate the bipolar contributions above T_{N}.

describing the phonon heat transport change with temperature, giving a net variation $\lambda_{\mathrm{ph}}(T)$. At low temperatures where $T \ll \theta = 224$ K (θ is the Debye temperature) phonons are scattered mainly by crystal boundaries, yielding the dependence $\lambda_{\mathrm{ph}} \propto T^3$. At $T > \theta$ the phonon–phonon scattering results in a temperature dependence $\lambda_{\mathrm{ph}} \propto T^{-1}$. At intermediate temperatures, i.e. for $T > T_{\mathrm{max}}$ (T_{max} is the temperature corresponding to the maximum in the phonon thermal conductivity), the phonon–phonon processes dominate, being of the Umklapp type (U processes), yielding the dependence $\lambda_{\mathrm{ph}} \propto \exp(\theta/\alpha T)$ [11]. However, any defects of the crystal or the presence of other phonon–phonon mechanisms in the heat transport leads to the deviation in the temperature dependences $\lambda_{\mathrm{ph}}(T)$ from those mentioned above. This is well apparent in figure 2. Especially at temperatures $T > 150$ K there is seen a departure from the dependence $\lambda_{\mathrm{ph}} \propto T^{-1.15}$: a strong increase of the thermal conductivity with increasing temperature. A similar change in the thermal conductivity is observed in semimetals at the moment of switching of the bipolar heat transport [12]. Assuming that electrons and holes are scattered independently of each other and that their relaxation time is $\tau \sim \varepsilon^r$, and taking into account the parabolic bands, one can derive the bipolar contribution of the thermal conductivity, λ_{bip}. This quantity is described as follows:

$$\lambda_{\mathrm{bip}} = T\left(\frac{k_0}{e}\right)^2 \left\{ \frac{A_n}{\rho_n} + \frac{A_p}{\rho_p} + \frac{1}{\rho_n + \rho_p}\left[\delta_n + \delta_p - \frac{\varepsilon_0}{k_0 T}\right]^2 \right\} \tag{2}$$

where k_0 is the Boltzmann constant, ρ_n and ρ_p are the electrical resistivities of both kinds, i.e. electrons and holes, ε_0 is the energy of overlapped bands (see the inset of figure 3),

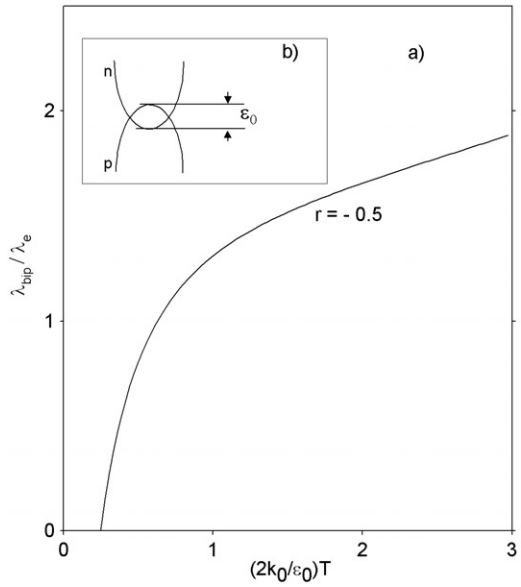

Figure 3. Temperature dependence of the ratio λ_{bip}/λ_e (equation (5)) for $r = -0.5$ (acoustic phonons). The inset displays the electronic band scheme for semimetals.

$$\delta_{n,p} = \frac{[(r+5/2)F_{r+3/2}(\mu^*_{n,p})]}{[(r+3/2)F_{r+1/2}(\mu^*_{n,p})]}, \tag{3}$$

$$A_{n,p} = \frac{(r+7/2)F_{r+5/2}(\mu^*_{n,p})}{(r+3/2)F_{r+1/2}(\mu^*_{n,p})} - \frac{(r+5/2)^2F^2_{r+3/2}(\mu^*_{n,p})}{(r+3/2)^2F^2_{r+1/2}(\mu^*_{n,p})}, \tag{4}$$

$F_r(\mu^*)$ is the Fermi integral, r is a factor describing the dependence of relaxation time of heat carriers carrying heat on the phonon energy, $\mu^*_n = E_F/k_0T$, $\mu^*_p = (\varepsilon_0 - E_F)/k_0T$, and E_F is the Fermi energy. Calculation of the bipolar contribution from expressions (2) to (4) is difficult due to the lack of the possibility to determine all the parameters occurring in these expressions. However, it is possible if one assumes some simplification, such as $\rho_p = \rho_n$ and that the effective of masses of electrons and holes are equal, $m^*_n = m^*_p$ (actually $m^*_p \gg m^*_n$), the Fermi energy $E_F = \varepsilon_0/2$, $\mu^*_p = \mu^*_n$, $\delta_n = \delta_p = \delta$, and $A_n = A_p = A$. Then, according to [12], the ratio between the bipolar and electron conductivities is given by

$$\lambda_{bip}/\lambda_e = \frac{(\delta - \varepsilon_0/2k_0T)^2}{A}. \tag{5}$$

For $r = -0.5$, i.e. where we are concerned only with the scattering on phonons, expression (5) gives the dependence presented in figure 3. From the data of figure 1 (values of λ_e) and those in figure 2, it is possible to calculate the temperature dependence $\lambda_{bip}(T)$, and the obtained data are presented in figures 4. The long dashed line presents the results which have been determined from the experimental data of the electron thermal conductivity for different magnitudes of ε_0 given in figures 4(a) and (b). The black circles displayed in these figures mark the calculated bipolar thermal conductivity taken as the difference between the differential curves $\Delta(\lambda_{tot} - \lambda_e)$ and by the interpolated dot–dashed and dashed lines, depending on the measured direction, shown in figure 2.

Within the temperature range 160–300 K, the ε_0 values are found to be of about one order of magnitude larger along the c direction than those estimated in the ab plane. Such an

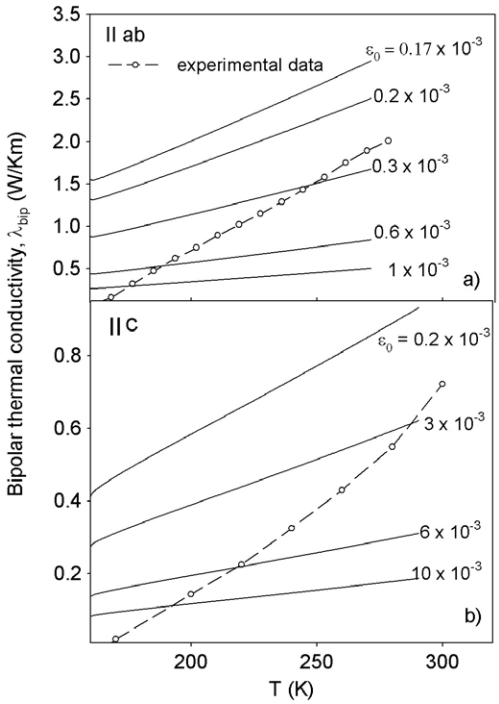

Figure 4. Bipolar thermal conductivity λ_{bip} extracted from the experiment (dashed curve) and compared to calculated values for different magnitudes of energy for two cases: when the temperature gradient was applied (a) perpendicular and (b) parallel to the *c* axis.

anisotropy in ε_0 may originate from the difference in the degree of the degeneration of electron gas μ_n^* along these two crystallographic directions. It is well known that one can estimate μ_n^* directly from the thermoelectric power $S(T)$ [7]. Thus in the work [13] the $S_i(T)$ dependences measured parallel and perpendicular to the *c* axis were given for the same single crystals. The ratio $S_\perp/S_\parallel \cong 20$ determined for $T > T_{\mathrm{N}}$ confirms the high anisotropy observed by us in ε_0.

It is obvious that the difference in slope of the curves describing the bipolar thermal conductivity and of those calculated from the electronic thermal conductivity content ($\lambda_{\mathrm{e}} = L_0 T/\rho$) is probably caused by not taking into account other resistivity features, like, for example, scattering of heat carriers on the disordered spins, or it may be also a result of the fact that below the ordered temperature the contributions into the thermal conductivity are originated not only by phonons but also by magnons (note the assumptions given above from which expression (5) has been derived).

Usually the theoretical analysis of the lattice thermal conductivity is based on the Debye model in which λ_{ph} is a function of the inverse relaxation time τ_i:

$$\lambda_{\mathrm{ph}} = GT^3 \int_0^{\Theta/T} \frac{x^4}{\tau^{-1}\sinh^2(x/2)}\mathrm{d}x \tag{6}$$

where $x = h\omega/k_0T$, G is constant, and τ^{-1} is the sum of inverse relaxation times for various phonon scattering processes: $\tau^{-1} = \Sigma\tau_i^{-1}$, where $\tau_i = \tau_{\mathrm{d}}, \tau_{\mathrm{pd}}, \tau_{\mathrm{U}}$ are relaxation times for the phonon scattering on dislocations, point defects and impurities, and finally a Umklapp phonon–phonon processes, respectively. The relaxation time can be expressed by a function dependent on the frequency ω for a particular scattering process τ_i [11]: $\tau_{\mathrm{d}}^{-1} = C_1\omega$—dislocations,

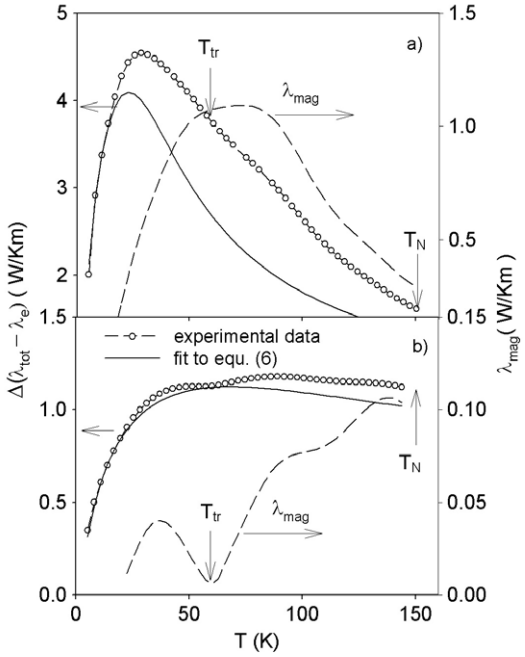

Figure 5. The difference $\Delta(\lambda_{tot} - \lambda_e)$ derived for two cases where the gradient is applied (a) within the *ab* plane and (b) parallel to the *c* axis both as a function of temperature: experiment (open circles: left-hand scale) and fitting to equation (6) (solid curve: left-hand scale) as well as the derived magnon part of the thermal conductivity (long dashed curves:-right-hand scale).

Table 2. Parameters of fittings of equation (6) to the experimental data.

Crystallographic axes	c_1	c_2 (s^3)	c_3 (s)	a (K)	v ($m\ s^{-1}$)	Θ (K)
c	2.2×10^6	9.0×10^3	7.5×10^6	75	6000	224
ab	3.7×10^6	8.5×10^5	1.4×10^7	70	6000	224

$\tau_{pd}^{-1} = C_2\omega^4$—point defects, and $\tau_U^{-1} = C_3\omega^2 T \exp[-a/T]$—Umklapp processes. Taking into account the Debye temperature $\theta = 224$ K [8] and a mean value of sound velocity for the material with a similar density to that of the investigated sample, i.e. $v_{ph} \approx 6000$ m s^{-1} [14], as well as the functions dependent on ω, for different τ_i values, we have made fits of expression (6) to the experimental data of the difference $\Delta(\lambda_{tot} - \lambda_e)$ (see in figures 5(a) and (b) the curves measured within the *ab* planes and those along the *c* directions, respectively). Table 2 gives the obtained parameters of the least squares fitting of experimental data to equation (6).

For the assumed values of sound velocity and Debye temperature, we have found a good agreement of the experimental data with equation (6) in the range of low temperatures where a domination of phonon scattering on point defects, impurities and dislocations takes place. On the other hand, at temperatures above 50 K, where we took into consideration only the Umklapp processes, the fitting curve lies below the experimental values. The reason for this is not taking into account another mechanism of phonon scattering (e.g. phonon–electron) as well as the presence of other mechanisms of the heat transport apart from the phonon ones. In magnetically ordered materials such an additional mechanism is the magnon heat transport. Hence the difference $\Delta(\lambda_{tot} - \lambda_e)$ certainly contains below T_N the contribution of magnons, but

of course it is difficult to estimate exactly to what extent this is, having in mind the possible other contributions mentioned above. However, to simplify this problem we have assumed that this difference is just the magnon contribution.

In figures 5(a) and (b) the dashed line represents the derived magnon thermal conductivity λ_{magn}, below the ordering temperature. This kind of contribution was found from the difference between the experimental curves (open circles) and the fit to expression (6) (solid lines) calculated within the *ab* plane and along the *c* axis, respectively. The derived magnon part of the conductivity within the *ab* plane (figure 5(a)) increases with increasing temperature, achieving a broad maximum centred at about 80 K with a value of about 1 W K^{-1} m^{-1}. Then, it diminishes to zero at about 20 K. On the other hand, the maximum value of about 0.1 W K^{-1} m^{-1} (about 10%) of the difference $\Delta(\lambda_{tot} - \lambda_e)$ was found near T_N for the magnon part of the conductivity derived for the *c* direction (figure 5(b)). On lowering the temperature, this part of λ^{ab}_{magn} decreases to almost zero in the vicinity of 64 K and below this temperature it starts to grow and goes through a maximum at 38 K with a value of 0.04 W K^{-1} m^{-1}, and finally vanishes around 25 K. It is worthwhile noting that at temperatures close to 64 K where the *ab* part of $\lambda_{magn}(T)$ reaches its maximum, there occur anomalies in the temperature dependence of the susceptibility, heat capacity, thermoelectric power, electrical resistivity and Hall coefficient, probably associated with the reorientation of the magnetic moments, as have been reported (in [7]). It is also interesting to point out that only the part of the thermoelectric power measured perpendicularly to the *c* axis, i.e. within the *ab* plane, exhibits a very distinct minimum in $S_\perp(T)$ around this temperature, compared to the almost negligibly small cusp apparent near this temperature along the *c* axis.

4. Conclusions

Previous numerous investigations of $UNi_{0.5}Sb_2$ have indicated a set of interesting physical properties of this compound. In the present work we have measured the heat transport in both states, namely in the magnetically ordered state and in the paramagnetic one. Among others, the work demonstrates the influence of the change in the magnetic structure on the total thermal conductivity and large its anisotropy as inferred from the measurements performed within the *ab* plane and along the *c* axis. Furthermore, we have carried out some attempts to extract from the total thermal conductivity the temperature dependences of the electronic, bipolar and magnon parts of the thermal conductivity. For example, the estimated value of the energy ε_0 from the bipolar dependence shows that $UNi_{0.5}Sb_2$ is a semimetal. The magnon part of the thermal conductivity differs in magnitude and in the temperature dependences depending on the direction of the measurements. As to the last aspect it would be interesting to measure the thermal conductivity of the reference non-magnetic compound with the same crystal structure, if of course such a compound exists at all.

Acknowledgments

Financial support of KBN to grants (No 2 P03B 109 24) and (No 3 T08A 054 26) is acknowledged. The authors are grateful for a stimulated discussion with Professor I A Smirnov from Ioffe Physico-Technical Institute, St Petersburg and Professor B Coqblin from the Orsay University.

References

[1] Brylak M, Möller M H and Jeitschko W 1995 *J. Solid State Chem.* **115** 305
[2] Kaczorowski D 1992 *J. Alloys Compounds* **186** 333

[3] Kaczorowski D, Kruk R, Sanchez J P, Malaman B and Wastin F 1998 *Phys. Rev.* B **58** 9227
[4] Aoki D, Wiśniewski P, Miyake K, Watanabe N, Settai E, Yamamoto E, Haga Y and Onuki Y 1999 *J. Phys. Soc. Japan* **68** 2182
[5] Ikeda S, Tokiwa Y, Okubo T, Yamada M, Tatsuma D, Inada Y, Settai R, Yamamoto E, Haga Y and Onuki Y 2003 *Physica* B **329–333** 610
[6] Bukowski Z, Kaczorowski D, Stępień-Damm J, Badurski D and Troć R 2004 *Intermetallics* **12** 1381
[7] Bukowski Z, Gofryk K, Plackowski T and Kaczorowski D 2005 *J. Alloy Compounds* **400** 33
[8] Plackowski T, Kaczorowski D and Bukowski Z 2005 *Phys. Rev.* B **72** 184418
[9] Jeżowski A, Mucha J and Pompe G 1987 *J. Phys. D: Appl. Phys.* **201** 1500
[10] Mucha J, Dorbolo S, Bougrine H, Durczewski K and Ausloos M 2004 *Cryogenics* **44** 145
[11] Berman R 1976 *Thermal Conduction in Solids* (Oxford: Clarendon)
[12] Golubkov A V, Parfienieva L S, Smirnov J A, Misiorek H, Mucha J and Jeżowski A 2000 *Phys. Solid State* **42** 1357
[13] Madelung O 1957 *Handb. Phys.* **20** 58
[14] Samsonov G V (ed) 1968 *Handbook of the Physicochemical Properties of the Elements* (New York: IFI Plenum)